# Experimental Demonstration of the Wave-Particle Duality of Electrons through Investigation of Atomic Separation of Graphene and Electron Charge-Mass Ratio

Gonghan Xu, Curtis Stephens

Two experiments were carried out to demonstrate the wave-particle duality of electrons while measuring the inter-atomic spacing of graphene and the electron charge-mass ratio. Both the wave and the particle properties of electron were testified. The inter-atomic distance of graphene was determined to be 1.3Å and the electron charge-mass ratio was determined to be $1.6 \times 10^{11}$C/kg. These results do not align with the published values perfectly, but the deviations are in general reasonable given the experimental conditions.

## 1 Introduction

A century after Thomas's Young's double-slit experiment which clearly demonstrated the wave nature of light[1] and eighteen years after Heinrich Hertz's experimental confirmation of light as an electromagnetic radiation,[2] Einstein proposed in 1905 that light must have a particle aspect in order to explain the photo-electric effect.[3] Einstein's theory established the wave-particle duality of light, which inspired Louis V. de Broglie to propose in his 1924 doctoral thesis that particles should also exhibit properties of wave and that the wavelength of a particle is related to its momentum.[4] De Broglie's hypothesis did not take long to get confirmed. Between 1925 and 1927, Clinton J. Davisson and Lester H. Germer, while scattering electrons from various materials to study the properties of metallic surfaces at Bell Telephone Laboratory, accidentally confirmed the de Broglie wavelength of electrons from their electron scattering patterns.[5] Shortly after Davisson and Germer reported their results, George P. Thomson, son of J. J. Thomson, also reported seeing effects of electron diffraction.[6] These experiments testified de Broglie's theory of matter waves. De Broglie collected his Nobel Prize in 1929 "for his discovery of the wave nature of electrons".[7] Davisson and Thomson also shared the Nobel Prize in Physics in 1937 for their experimental work on electron diffraction.[8]

As undergraduate students, we carried out two experiments to verify the wave-particle duality of electrons. In the first experiment, we used graphite to scatter electrons and determine the carbon-carbon separation in a graphene layer. This experiment should demonstrate the wave characteristic of electrons. In the second experiment, we observed circular motions of thermionically emitted electrons in a nearly uniform magnetic field and determined the electron charge-mass ratio. This experiment was intended to demonstrate the particle nature of electrons.

## 2 Theory

This section will describe theories that are relevant to the two experiments.

## 2.1 De Broglie wavelength

From Plank's quantum theory and Einstein's special relativity, the energy of a photon can be expressed as

$$E = hf = pc \tag{1}$$

where h is the Plank constant, f is the frequency of the photon, p is the magnitude of the photon's momentum, and c is the speed of light. Therefore, for a photon, we have $h = \frac{c}{f}p = \lambda p$, where $\lambda$ is the wavelength of the photon. De Broglie extended this result to all particles. So, the de Broglie wavelength of a matter wave should obey

$$\lambda = \frac{h}{p} \tag{2}$$

where p is the magnitude of the particle's momentum.[4]

## 2.2 Bragg's law

To understand electron diffraction and Bragg's law, it is necessary to understand x-ray diffraction first with a little historical background.

Soon after Max Von Laue successfully performed his x-ray diffraction experiments with two of his colleagues in 1912,[9] William Lawrence Bragg proposed an alternative explanation that simplifies Laue's original analysis. Figure 1(a) is a schematic diagram of Laue's diffraction experiment. As shown in the figure, when

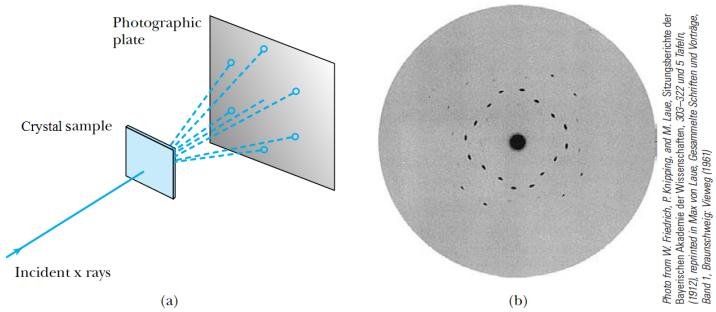


Figure 1: (a) Schematic diagram of Laue's x-ray diffraction experiment (b) One of the first results of Laue's experiments showing the symmetric placements of dots of x-ray scattered from ZnS

a beam of x-ray is emitted toward a crystal sample, the beam will be scattered from the crystal sample and produce dots (Laue dots) on the photographic plate. Figure 1(b) shows the Laue dots in one of the first results of Laue's experiments. According to W.L. Bragg, each dot surrounding the central bright spot in Figure 1(b) can be interpreted as a constructive interference of the incident x-ray reflected from a unique set of lattice planes (Bragg planes) within the crystal.

As shown in Figure 2, a crystal, such as NaCl, can have many sets of Bragg planes. There is a interplanar distance $d_i$ for each set of planes. Figure 3 shows a schematic diagram of x-ray scattering from a set of Bragg planes of a crystal. As shown in the figure, for the two monochromatic x-ray beams to interfere constructively, they must go through distances that differ by multiples of the x-ray's wavelength. Therefore, Bragg proposed his law

$$n\lambda = 2d\sin\theta \tag{3}$$

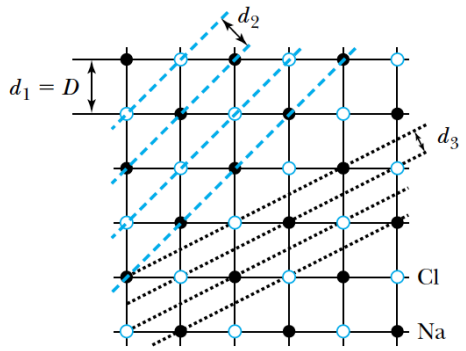


Figure 2: Top view of NaCl with possible Bragg planes. D is the inter-atomic spacing and $d_i$ are the inter-Bragg plane spacings.

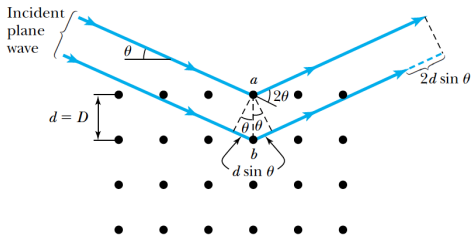


Figure 3: Schematic diagram of x-ray scattering from Bragg planes

that must be satisfied for x-rays to interfere constructively at the Laue dots. In Equation 3, as illustrated in Figure 3, the positive n is called the order of reflection, $\lambda$ is the wavelength of the incident monochromatic x-ray, d is the inter-Bragg plane spacing, and $2\theta$ is the scattering angle.[10]

Since electrons can also behave like waves, electrons, when emitted to a single large crystal, will produce similar interference pattern as that in Figure 1(b). Bragg's law applies to electron diffraction as well.[11]

## 2.3 Powder diffraction

As discussed in Section 2.2, a single large crystal will scatter electrons into dots on a receiving screen. If many small crystals, grounded into a powder form, are used as the scatterer instead, then the interference pattern of the electrons will be a series of fringe rings. This is because the small crystals in the crystal powder will have random orientations so that the interference pattern will be azimuthally symmetric with respect to the incidence electron beam.[12]

## 2.4 The structure of graphite

As illustrated in Figure 4, a graphite crystal consists of a stack of flat layers of carbon atoms. In each layer (called a graphene plane), the carbon atoms are arranged in a hexagonal structure like a honeycomb with equal distances between neighboring carbons.[13]

Bragg planes of graphite need to be determined from the crystal's unit cells and lattice vectors, which

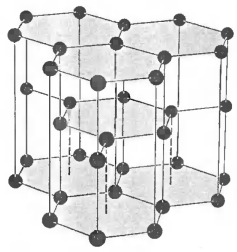

Figure 4: The structure of graphite

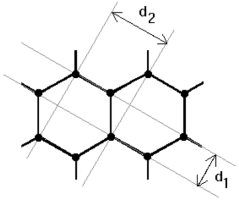


Figure 5: The two smallest inter-Bragg plane spacings of graphite

will not be elaborated here. Figure 5 shows the two smallest inter-Bragg plane spacings of graphite.[14] In the figure, suppose the inter-carbon distance in a graphene layer is $a_0$, then we can determine that $a_0 = \frac{2}{\sqrt{3}}d_1 = \frac{2}{3}d_2$ and $\frac{d_2}{d_1} = \sqrt{3}$ from the hexagonal geometry.

### 2.5 Lorentz force

A charged particle moving in an electromagnetic field will experience an electromagnetic force, called the Lorentz force. Suppose the charge of the particle is q, the electric field and the magnetic field at the position of the particle are $\vec{E}$ and $\vec{B}$ respectively, and the velocity of the particle is $\vec{v}$, then the electromagnetic force on the charged particle is[15]

$$\vec{F} = q(\vec{E} + v \times \vec{B}) \tag{4}$$

For an electron of charge -e with an initial velocity $\vec{v}$ perpendicular to a background uniform magnetic field $\vec{B}$, the Lorenz force is

$$F = evB \tag{5}$$

where F, v, and B denote the magnitudes of the respective vector quantities. This force is always perpendicular to the velocity of the electron so that the electron will move in a uniform circular motion.

## 3 Experiment

This investigation consists of two parts. The first part, the electron diffraction experiment, aims at determining the inter-atomic spacing of a graphene layer while demonstrating the wave property of electrons. The second part, the electron charge-mass ratio experiment, is intended for determining the charge-mass ratio of an electron while demonstrating electrons' particle property.

## 3.1 The electron diffraction experiment

### 3.1.1 Experimental setup

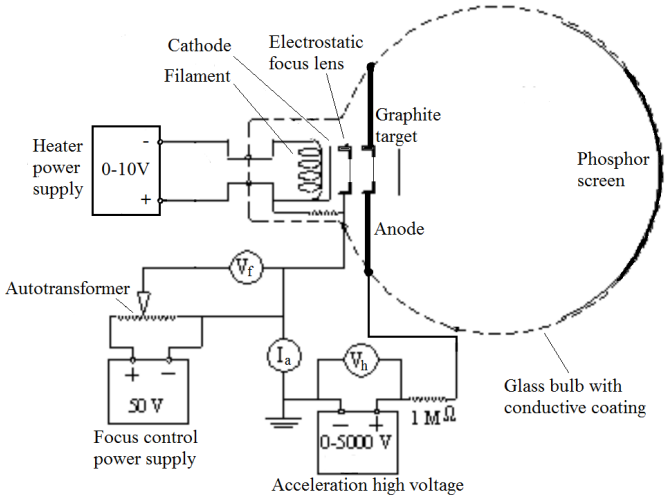


Figure 6: Experimental setup for the electron diffraction experiment

As shown in Figure 6, the electron diffraction experiment setup mainly consists of a glass bulb and three power supplies. In the glass bulb, from left to right as shown in Figure 6, is there a filament, an electron-emission cathode, an electrostatic lens, an anode electrode, a graphite target (comprised of graphite powder), and a phosphor screen (on the inner surface of the glass bulb). The filament is connected to a power supply (the heater power supply) and thus can be heated when the power supply is on. The heated filament will subsequently heat the electron-emission cathode, which will then emit electrons by thermionic emission[16]. The electrostatic lens is connected to the second power supply (the focus control power supply), which delivers a voltage that is adjustable by an autotransformer. The third power supply will provide a high voltage between the electrostatic lens and the anode so that electrons passing through the electrostatic lens will be accelerated toward the anode before hitting the graphite target. When the three power supplies are turned on and properly tuned, the electrons emitted by cathode will be focused onto the graphite powder and then be scattered by the powder onto the the glass bulb. When the scattered electrons hit the glass bulb, the phosphor screen will glow green as phosphorus atoms on the screen get excited by the electrons and subsequently emit photons before returning to their original states. A soft, bendable, scale is stuck on the outer surface of the glass bulb over the phosphor screen in order to measure the interference pattern of the electrons on the phosphor screen. The inner wall of the glass bulb is covered with a conductive coating so that electrons hitting the glass bulb will eventually be collected back to the anode. As shown in Figure 6, there is a milliammeter which monitors the current that flows through the anode. Besides, the negative terminals of the high voltage power supply and the focus control power supply are both grounded, and a voltmeter is used to monitor the autotransformer-adjusted focus control voltage.

### 3.1.2 Experimental theory

According to Section 2.2 and Section 2.3, the focused electron beams that hit the graphite target will be scattered onto the phosphor screen and display an interference pattern of bright and dark fringes as rings.

The radii of the bright fringe rings can be used to derive the scattering angle, which can in turn be used to calculate the inter-atomic spacing of graphene. As shown in Figure 7, let s be the curved radius of a bright

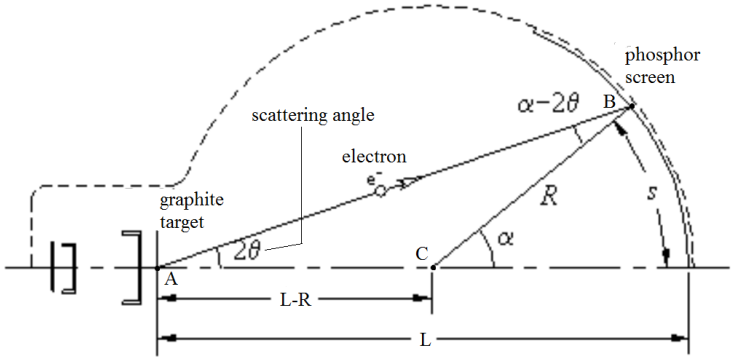


Figure 7: The scattering geometry for the electron diffraction experiment

fringe ring, R be the radius of the spherical part of the glass bulb, L be the horizontal distance between the graphite target and the other end of the glass bulb, and $\alpha$ be the central angle subtended by the curved ring radius s. Then we have

$$\alpha = \frac{s}{R} \tag{6}$$

Applying the law of sines in Triangle ABC, we have

$$\frac{\sin(\alpha - 2\theta)}{L - R} = \frac{\sin(2\theta)}{R} \tag{7}$$

With $\sin(\alpha - 2\theta) = \sin\alpha\cos 2\theta - \cos\alpha \sin 2\theta$ and $\alpha = \frac{s}{R}$, Equation 7 can be rearranged as

$$\tan(2\theta) = \frac{\sin\alpha}{L/R + \cos\alpha - 1} = \frac{\sin(s/R)}{L/R + \cos(s/R) - 1} \tag{8}$$

The values of L and R are provided with the experimental apparatus as 136.4±0.2mm and 64.2±0.1mm, respectively. Therefore, as long as the bright fringe ring radius $s$ is known, we can determine the scattering angle $2\theta$ from Equation 8.

From Section 2.2, we know that the scattering angle corresponding to a bright fringe ring can be related to the inter-Bragg plane spacing $d$ of the graphite target by Bragg's law. From Equation 3, we have $d = \frac{n\lambda}{2\sin\theta}$. If we assume the order of reflection n is one (since larger n will correspond to larger fringe rings that are hardly accommodable by the phosphor screen), then we have

$$d = \frac{\lambda}{2\sin\theta} \tag{9}$$

Therefore, in order to obtain the inter-Bragg plane spacing d, we need to know the wavelength of the incident electrons as well as the scattering angle. From Equation 2, we know that the wavelength of an electron is related to its momentum. As shown in Figure 6, the electrons are accelerated from the electrostatic lens to the anode electrode by a high voltage. Let the high voltage be $V_h$, then an electron, during the acceleration process, will gain a kinetic energy of $\Delta KE = eV_h$, where e is the magnitude of the electron charge. Assume the temperature of the filament is on a scale of T=3000K, then the initial kinetic energy of a typical electron

emitted by the cathode is on a scale of $kT = 0.26\text{eV}$, where $k = 1.38 \times 10^{-23} J/K$ is the Boltzmann constant. In this experiment, the high acceleration voltage is on a scale of 1000 volts, so we have $\Delta KE = eV_h \sim 1000\text{eV}$. Therefore, the initial kinetic energy of a typical emitted electron is negligible compared to the gained kinetic energy due to the acceleration voltage, and hence we can take $eV_h$ as the final kinetic energy of an electron. Notice that the rest mass energy of an electron is about 0.5MeV, which is two orders of magnitude larger than $eV_h \sim 1000\text{eV}$. Therefore, we can use the non-relativistic limit in our calculations for the electrons. In the non-relativistic limit, an electron's kinetic energy is related to its momentum

$$\text{KE} = \frac{p^2}{2m} \tag{10}$$

where m is the rest mass of an electron and p is the magnitude of the electron's momentum. Therefore, we have $p = \sqrt{2\,\text{KE}\,m} = \sqrt{2eV_h m}$. From Equation2, we can obtain the electron's wavelength as

$$\lambda = \frac{h}{p} = \frac{h}{\sqrt{2eV_h m}} \tag{11}$$

where h is the Plank constant. Plugging Equation 11 into Equation 9, we have

$$d = \frac{h/\sqrt{2eV_h m}}{2\sin\theta} \tag{12}$$

Since $\theta$ and $V_h$ are both measurable quantities in this experiment, the inter-Bragg plane spacing d of graphite can be obtained. Equation 12 can be rearranged as

$$\sin\theta = \frac{h}{d\sqrt{8em}} \frac{1}{\sqrt{V_h}} \tag{13}$$

In this experiment, we would vary the acceleration voltage $V_h$ and obtain the corresponding half-scattering angles $\theta$ for the bright fringe rings from Equation 8. Thus, with multiple data points of $V_h$ and $\sin\theta$, we can use linear fitting to obtain an average inter-Bragg plane spacing $d_i$ for each bright fringe ring from Equation 13. According to Section 2.4, the inter-Bragg plane spacings $d_i$ can then be used to infer the inter-atomic spacing $a_0$ of graphene.

### 3.1.3 Procedure

The heater power supply was initially turned on to 6 volts, and we waited about one minute for the filament to heat up. Then, the focus control power supply was turned on and was adjusted to 25 volts with the autotransformer. The high voltage power supply was also turned on to an initial voltage of 1500 volts. After this, the light of the laboratory was turned off and we observed two concentric, bright, green fringe rings on the phosphor screen. Since each ring has an internal width, for each ring, we read and recorded the lengths of its inner diameter as well as its outer diameter. Then we increased the acceleration voltage by 250 volts, and read and recorded the lengths of the inner and outer diameters of the two rings again. This process was repeated until the acceleration voltage reached 5000 volts, and a total of 15 acceleration voltages and the corresponding four diameters were recorded. During the process of varying the acceleration voltage, caution was used to prevent the anode current from exceeding 0.2mA so that the electron beam would not be too intense to damage the the graphite target or decrease the lifetime of the cathode. To keep the anode current below 0.2mA, the heater voltage was lowered to 5 volts for the 1750 volts acceleration voltage and 4.5 volts for all subsequent acceleration voltages.

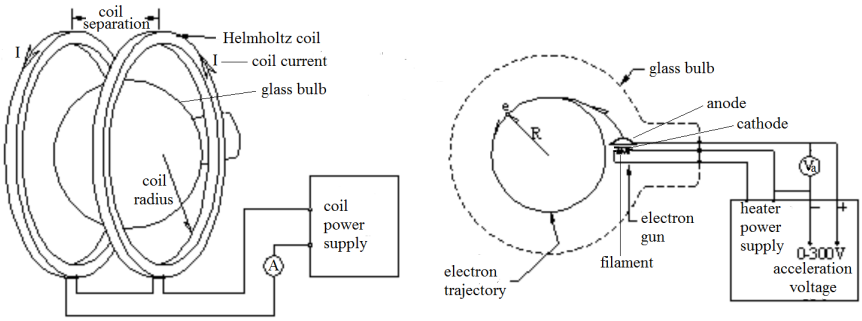


Figure 8: Experimental setup for the charge-mass ratio experiment

## 3.2 The electron charge-mass ratio experiment

### 3.2.1 Experimental setup

As shown in Figure 8, the setup of this experiment mainly consists of a glass bulb and a Helmholtz coil. Inside the glass bulb, there is an electron gun which is comprised of a filament, an indirectly heated cathode electrode, and an anode electrode. A power supply (the heater power supply) is connected to the filament so that the filament can be heated when the power supply is on. Like in the electron diffraction experiment, the heated filament will in turn heat the cathode electrode, which will consequently emit electrons through thermionic emission. Another power supply (the acceleration voltage power supply) is used to provide a voltage between the cathode and the anode so that the emitted electrons from the cathode can be accelerated toward and go through the anode in a beam. The glass bulb contains argon with properly-adjusted pressure so that the trajectory of the electron beam can be visible when the light of the laboratory is turned off, due to excitation of the argon atoms by the electrons. As shown in Figure 8, the glass bulb is placed inside the Helmholtz coil, with a coil radius of 15cm and a coil separation of 15cm. In each part of the two coils, there are 130 turns of wire. The Helmholtz coil is connected to a third power supply (the coil power supply). When this power supply is on, the Helmholtz coil will produce a nearly uniform magnetic field between the two coils. A milliammeter is installed in the circuit of the Helmholtz coil to monitor the coil current. A voltmeter is attached to the acceleration voltage power supply to monitor the acceleration voltage.

### 3.2.2 Experimental theory

In this experiment, the speeds of the electrons will lie in the non-relativistic regime because the acceleration voltages were kept below 300 volts (note the higher acceleration voltages applied in the electron diffraction experiment that would still keep the electrons non-relativistic). Therefore, only non-relativistic equations will be used in this section.

According to Section 2.5, an electron moving in a uniform magnetic field will experience a Lorentz force, which is always perpendicular to the electron's velocity. When the magnetic field is perpendicular to the initial velocity of the electron, the Lorentz force will act as a constant centripetal force so that the electron will conform to a uniform circular motion. Suppose the initial speed of an electron is v, the magnitude of the uniform magnetic field is B, and the electron charge is -e. Then according to Equation 5, the Lorentz force on the electron with an initially velocity perpendicular to the magnetic field is

$$F = evB \tag{14}$$

Since this force F is also the centripetal force on the electron, we can write this force as

$$F = \frac{mv^2}{R} \tag{15}$$

where m is the electron rest mass and R is the radius of the circular trajectory of the electron. Remember that the speed of the electron will not change during this circular motion. Combining Equation 14 and Equation 15 and eliminating F, we can obtain

$$\frac{e}{m} = \frac{v}{BR} \tag{16}$$

Therefore, the charge-mass ratio of an electron can be determined as long as we know its initial speed, the magnitude of the magnetic field, and the radius of the electron trajectory. In this experiment, the radius of the electron trajectory can be measured. The magnitude of the magnetic field is related to the current through the Helmholtz coil by

$$B = \frac{8\mu_0 NI}{5\sqrt{5}R_{coil}} \tag{17}$$

where $\mu_0$ is the vacuum magnetic permeability, N is the number of turns of wire in each of the two coils, I is the coil current, and $R_{coil}$ is the radius of the Helmholtz coil.[17] The initial speed of the electron can be calculated from the electron's initial kinetic energy through the non-relativistic relation KE = $\frac{1}{2}mv^2$. Let the acceleration voltage be $V_a$, then using a similar argument as in Section 3.1.2, we can take $eV_a$ to be the initial kinetic energy KE of an electron just leaving the anode electrode. Therefore, we can relate the acceleration voltage with the initial speed of the electron: $eV_a = \frac{1}{2}mv^2$. Rearranging this equation, we have

$$\frac{e}{m} = \frac{v^2}{2V_a} \tag{18}$$

Combining Equation 18 and Equation 16 and eliminating $\frac{e}{m}$, we can obtain

$$v = \frac{2V_a}{BR} \tag{19}$$

Plugging Equation 19 back into Equation 16, we obtain

$$\frac{e}{m} = \frac{2V_a}{(BR)^2} \tag{20}$$

where the $V_a$, B, and R are all measurable quantities in this experiment.

### 3.2.3 Procedure

First, the heater power supply was turned on to supply a constant current of 0.83A to the filament. We waited for about one minute for the filament to heat up, and then turned on the acceleration voltage power supply to 170 volts. After this, the light of the laboratory was turned off and the visibility of an electron beam was confirmed. Then, the Helmholtz coil power supply was turned on and gradually increased until the electron trajectory closed around on itself as a circle. The acceleration voltage and the coil current were recorded. The diameter of the electron trajectory was also measured an recorded with a head-up display projection scale (HUD). This process was repeated for 13 combinations of the coil current and the acceleration voltage.

# 4 Data analysis

## 4.1 The electron diffraction experiment

For this experiment, we measured the inner and outer diameters of the two bright fringe rings (a small ring and a large ring) on the phosphor screen for 15 equally-spaced acceleration voltages from 1500 volts to 5000 volts. For each ring, I calculated not only its inner and outer radii, but also its central radius as an average of its inner and outer radii. For each of the three radii (inner, central, and outer) of each ring, I used Equation 8 to calculate the corresponding values of $\tan(2\theta)$ and hence those of $\sin\theta$ for the 15 acceleration voltages. For each ring and for each type of radius of the ring, I plotted the corresponding values of $\sin\theta$ vs. $\frac{1}{\sqrt{V_h}}$ and used linear fitting to find the corresponding average inter-Bragg plane spacing d based on Equation 13.

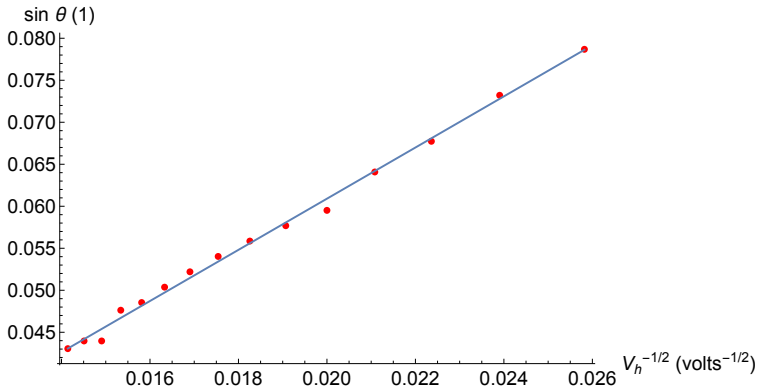


Figure 9: $\sin\theta$ vs. $\frac{1}{\sqrt{V_h}}$ for the central radius of the smaller bright fringe ring

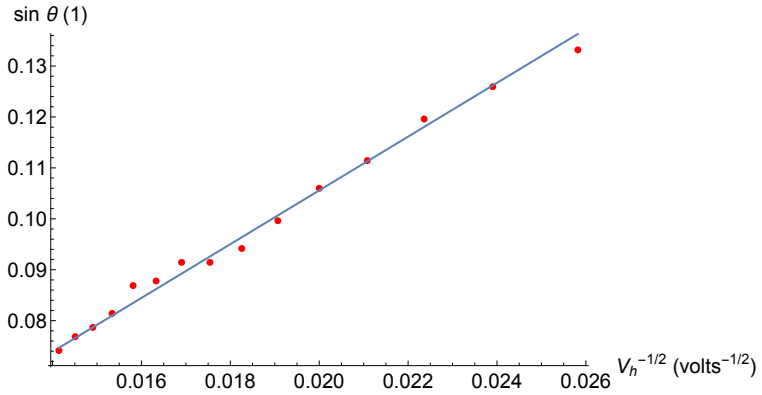


Figure 10: $\sin\theta$ vs. $\frac{1}{\sqrt{V_h}}$ for the central radius of the larger bright fringe ring

As shown in Figure 9 and Figure 10, the values of $\sin\theta$ vs. $\frac{1}{\sqrt{V_h}}$ for the central radii of the two rings are plotted respectively. According to Equation 13, for each plot, a linear line $\sin\theta = kV_h$ was used to fit the data points with Mathematica. The proportionality constant $k_{small}$ for the smaller ring is found to be 3.04511 volts$^{1/2}$, and $k_{large}$ for the larger ring is found to be 5.27882 volts$^{1/2}$. From Equation 13, we can calculate the

corresponding inter-Bragg plane spacings from $k_i$, by $d_i = \frac{h}{k_i\sqrt{8me}}$. Therefore, the corresponding inter-Bragg plane spacings for the smaller and the larger rings are calculated to be $d_{small} = 2.014$Å and $d_{large} = 1.162$Å. According to Section 2.4, we have $\frac{d_{small}}{d_{large}} = 1.733 \approx \sqrt{3}$, so we can confirm that the two bright fringe rings correspond to the two smallest inter-Bragg plane spacings of graphite. According to Section 2.4, the inter-atomic spacing of graphene is $a_0 = \frac{2}{3}d_{small} = \frac{2}{\sqrt{3}}d_{large}$. Therefore, we can calculate $a_0$ from the average of $\frac{2}{3}d_{small}$ and $\frac{2}{\sqrt{3}}d_{large}$, which is 1.3Å.

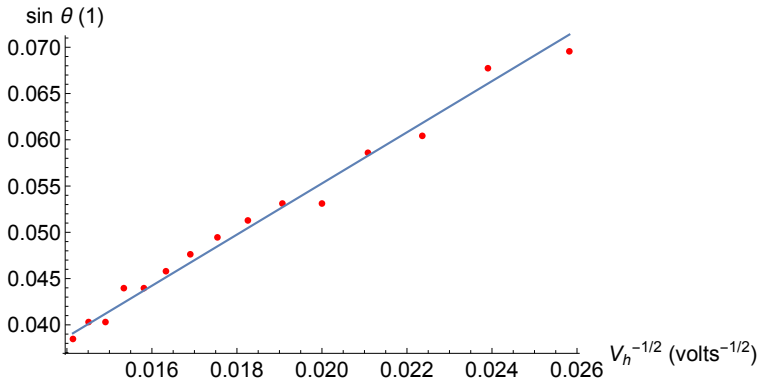


Figure 11: $\sin\theta$ vs. $\frac{1}{\sqrt{V_h}}$ for the inner radius of the smaller bright fringe ring

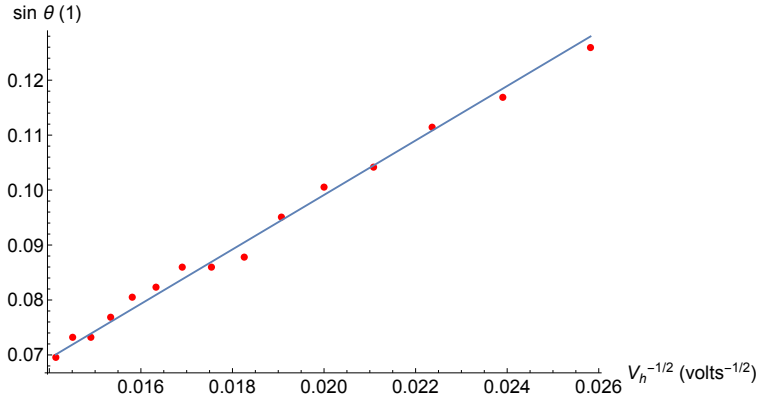


Figure 12: $\sin\theta$ vs. $\frac{1}{\sqrt{V_h}}$ for the inner radius of the larger bright fringe ring

Notice that this $a_0$ value is obtained from the central radii of the two rings. To obtain an uncertainty range for this value, we can use the corresponding data of the inner and outer radii of the two rings. As per Figures 11-14, using the same linear fitting method on the inner and outer radii, I obtained the corresponding inter-Bragg plane spacings to be $d_{small,inner} = 2.218$Å, $d_{large,inner} = 1.237$Å, $d_{small,outer} = 1.844$Å, and $d_{large,outer} = 1.095$Å. The corresponding average $a_0$ values are $a_{0,inner} = 1.5$Å and $a_{0,outer} = 1.2$Å. These can serve as upper and lower bounds for the $a_0$ value obtained from the central radius data. Therefore, we have found the inter-atomic spacing of graphene to be 1.3Å with an uncertainty of +0.2Å and -0.1Å. I only take two significant figures for $a_0$ because there are only two significant figures (accurate to 1mm) for the measured diameters of the bright fringe rings.

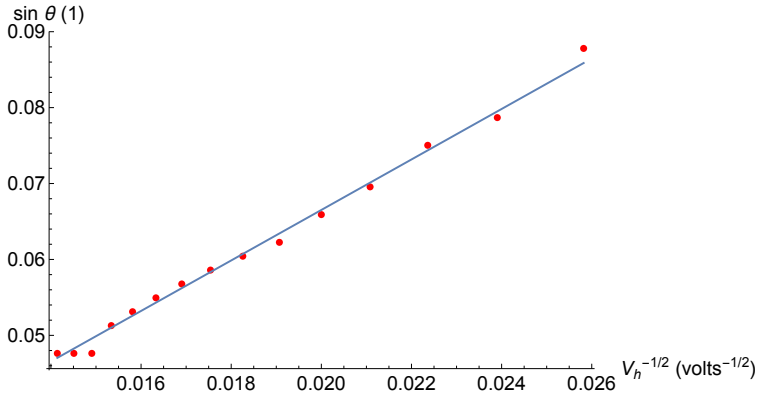


Figure 13: $\sin\theta$ vs. $\frac{1}{\sqrt{V_h}}$ for the outer radius of the smaller bright fringe ring

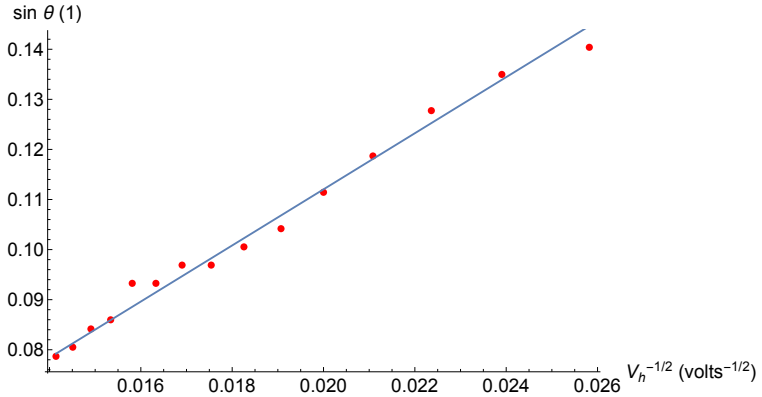


Figure 14: $\sin\theta$ vs. $\frac{1}{\sqrt{V_h}}$ for the outer radius of the larger bright fringe ring

### 4.2 The electron charge-mass ratio experiment

For this experiment, we recorded the acceleration voltages $V_a$, the coil currents $I$, and the electron trajectory diameters $D$ for 13 trials of different combinations of $V_a$ and $I$. Using Equations 17 and 20, for each trial, I obtained a corresponding value for the charge-mass ratio, as shown in Table 1. The average charge-mass ratio from results of all 13 trials is $1.6 \times 10^{11}$C/kg.

## 5 Conclusion

This investigation was intended to measure the inter-atomic spacing of graphene and the charge-mass ratio of an electron while demonstrating the wave-particle duality of electrons.

### 5.1 The electron diffraction experiment

The inter-atomic spacing of graphene was determined to be 1.3Å, with an uncertainty of +0.2Å and -0.1Å due to the internal width of the two bright fringe rings on the phosphor screen. The published value,

| Acceleration voltage (V) | Coil current (A) | Electron trajectory diameter (cm) | e/m (C/kg) |
|---|---|---|---|
| 170 | 1.2 | 9.8 | 1.6E+11 |
| 190 | 1.2 | 10.4 | 1.6E+11 |
| 220 | 1.3 | 10.4 | 1.6E+11 |
| 250 | 1.4 | 10.1 | 1.6E+11 |
| 220 | 1.4 | 9.6 | 1.6E+11 |
| 190 | 1.4 | 8.8 | 1.6E+11 |
| 170 | 1.4 | 8.2 | 1.7E+11 |
| 170 | 1.5 | 7.7 | 1.7E+11 |
| 190 | 1.5 | 8.3 | 1.6E+11 |
| 220 | 1.5 | 8.9 | 1.6E+11 |
| 250 | 1.5 | 9.5 | 1.6E+11 |
| 250 | 1.6 | 8.8 | 1.7E+11 |
| 250 | 1.7 | 8.3 | 1.7E+11 |

Table 1: Determined charge-mass ratios for the 13 trials of the charge-mass ratio experiment

1.42Å,[13] is about 9 percent larger than the determined value. However, the published value still lies in the uncertainty range of the experimentally determined value well. The deviation of the published value from the experimentally determined value is likely attributed to the difficulty in measuring the inner and outer diameters of the bright fringe rings accurately. In this experiment, the bright fringe rings displayed very vague boundaries from the surrounding darker regions, especially at lower acceleration voltages. The larger ring would display even fuzzier boundaries than the smaller ring. Therefore, there should be a ±2mm uncertainty for each reading of a diameter (±1mm for each end of the diameter). To estimate the resulting uncertainty from the inherent inaccuracy in reading the fringe ring diameters, we can look at Equation 12 and see that any small fractional error in $\sin\theta$ would lead to about the same fractional error in the inter-Bragg plane spacing d, and thus about the same fractional error in the inter-carbon spacing of graphene $a_0$, since $a_0$ is proportional to d. From Figures 9 and 10, we can see that the angle $\theta$ involved in this experiment is small enough so that we have $\sin\theta \approx \theta \approx \tan\theta$. Therefore, from Equation 8, we can see that any small fractional error in the numerator $\sin\alpha$ will lead to about the same fractional error in $\tan(2\theta)$, and thus about the same fractional error in $\sin\theta$, and finally about the same fractional error in $a_0$. Denote the measurement error in $\alpha$ by $\Delta\alpha$, then we have

$$\frac{\sin(\alpha+\Delta\alpha)}{\sin\alpha} = \frac{\sin\alpha\cos\Delta\alpha + \cos\alpha\sin\Delta\alpha}{\sin\alpha} = \cos\Delta\alpha + \sin\Delta\alpha\cot\alpha \approx 1 + \sin\Delta\alpha\cot\alpha \tag{21}$$

From Equation 6, we know that $\Delta\alpha = \frac{\Delta s}{R}$. Since the uncertainty for the ring diameter is 2mm, that for the ring radius s will be 1mm. Recall that the radius of the glass bulb is 64.2mm. Therefore, $\Delta\alpha = \frac{1}{64.2} = 0.0156$. Plug this value of $\Delta\alpha$ into Equation 21, and use a typical value of $\alpha$ of $\frac{20mm}{64.2mm} = 0.312$ in the same equation, we can obtain the fractional error of $\sin\alpha$ to be about 5 percent. Notice that the 5 percent fractional error is only a scale estimate since we used 20mm as the scale of the ring radius. From previous reasoning, we know that this 5 percent error will propagate to the determined value of the carbon-carbon distance in a graphene layer. Therefore, the actual 9 percent error, on the same scale of the 5 percent scale estimation, likely comes from the inherent inaccuracy in measuring the fringe ring diameters on the phosphor screen. Another problem that might also affect the accuracy of the final result would be the precision of measurements involved in this experiment. The diameters of the fringe rings could only be measured to an accuracy of 1mm from the bendable scale. As a result, the final value of $a_0$ could only be accurate to two significant figures. Therefore, the error of the final result could be enlarged due to this problem. To improve the result of the experiment, more advanced experimental apparatus should be utilized which could withstand a more

intense electron beam (so that the boundaries of the electron interference fringes are more clearly visible) and measure the diameters of the bright fringe rings to a higher accuracy (so that the overall precision of the final result can be improved).

In this experiment, both the particle nature and the wave nature of electrons are demonstrated. When we tried to calculate the kinetic energy and the momentum of an electron reaching the graphite target, we were treating the electron like a particle. When we used De Broglie's relation (Equation 2) and the interference pattern of the electrons to figure out the carbon-carbon distance in graphene, we were relying on the wave property of electrons.

### 5.2 The electron charge-mass ratio experiment

In this experiment, the charge-mass ratio of an electron was found to be $1.6 \times 10^{11}$C/kg. The corresponding published value is $1.76 \times 10^{11}$C/kg.[18] Therefore, the published value is larger than the experimentally determined value by 10 percent. As in the electron diffraction experiment, one source of the experimental error is likely attributed to the level of precision involved in this experiment. From Equation 17 and Equation 20, we can write the charge-mass ratio as proportional purely to measurable quantities:

$$\frac{e}{m} \propto \frac{V_a}{(IR)^2} \tag{22}$$

Since both the coil current and the electron trajectory radius were in general measured up to two significant figures, the final results of the charge-mass ratio are bound to two significant figures. Therefore, the actual experimental error could be enlarged from this cause. Another major cause of the experimental error, like in the electron diffraction experiment, is the inherent inaccuracy in measuring the electron trajectory diameter. The electron trajectory in this experiment did not display a very clear boundary from the surrounding, and the trajectory was further dimmed as the electron beam moved away from the electron gun. As a consequence, each reading of the electron trajectory diameter could have a maximum uncertainty of 4mm (2mm for each end of the diameter). The typical diameter scale in this experiment is 100mm. Therefore, the 4mm uncertainty corresponds to a fractional uncertainty of $\frac{4mm}{100mm} = 4$ percent in the diameter and hence the radius, of the electron trajectory. Notice, from Equation 22, that the charge-mass ratio is inversely proportional to the square of the electron trajectory radius. Therefore, the 4 percent uncertainty would lead to a final uncertainty in the charge-mass ratio of about 8 percent. Together with the significant figure problem, which could enlarge the final uncertainty by $\frac{0.05}{1.76} \approx 3$percent, the 10 percent uncertainty was somehow explainable. However, from Table 1, the experimentally determined charge-mass ratios for all 13 trials were consistently lower than the published value, but an uncertainty from the difficulty of measuring the diameters accurately and the inherent precision level of the experimental apparatus should, at least occasionally, lead to results larger than the published value. Since the only human-measured quantities in this experiment are the diameters of the electron trajectory, it seems that, according to Equation 22, these diameters were measured consistently higher than the actual values. To find out the real cause of the errors involved, more trials of this experiment should be carried out carefully to see whether the obtained charge-mass ratios still turn out consistently lower than the published value.

In this experiment, the particle nature of electrons is demonstrated. Electrons are treated and analyzed as charged particles in calculating their initial speed at the end of the electron gun and in relating their circular motion to the background magnetic field.

## References

[1]J. Cutnell and K. Johnson, *Physics*, 9th ed. (Wiley, Hoboken, NJ, 2012), p. 838.

[2]S. T. Thornton and A. Rex, *Modern physics for scientists and engineers* (Cengage Learning, Boston, MA, 2012), p. 102.

[3]J. Cutnell and K. Johnson, *Physics*, 9th ed. (Wiley, Hoboken, NJ, 2012), pp. 897–901.

[4]S. T. Thornton and A. Rex, *Modern physics for scientists and engineers* (Cengage Learning, Boston, MA, 2012), pp. 168–169.

[5]R. K. Gehrenbeck, Physics today **31**, 34–41 (1978).

[6]S. T. Thornton and A. Rex, *Modern physics for scientists and engineers* (Cengage Learning, Boston, MA, 2012), p. 174.

[7]*The nobel prize in physics 1929*, `https://www.nobelprize.org/nobel_prizes/physics/laureates/1929/`.

[8]*The nobel prize in physics 1937*, `https://www.nobelprize.org/nobel_prizes/physics/laureates/1937/`.

[9]M. Eckert, Annalen der Physik **524** (2012).

[10]S. T. Thornton and A. Rex, *Modern physics for scientists and engineers* (Cengage Learning, Boston, MA, 2012), pp. 163–165.

[11]S. T. Thornton and A. Rex, *Modern physics for scientists and engineers* (Cengage Learning, Boston, MA, 2012), pp. 172–175.

[12]S. T. Thornton and A. Rex, *Modern physics for scientists and engineers* (Cengage Learning, Boston, MA, 2012), pp. 166–167.

[13]D. R. Cooper, B. D'Anjou, N. Ghattamaneni, B. Harack, M. Hilke, A. Horth, N. Majlis, M. Massicotte, L. Vandsburger, E. Whiteway, et al., ISRN Condensed Matter Physics **2012** (2012).

[14]S. Shelley and S. A. Kane, *Electron diffraction*, (2005) `https://ww3.haverford.edu/physics/Amador/documents/06bLEED.doc`.

[15]D. Griffiths, *Introduction to electrodynamics*, 4th ed. (Pearson Education, Glenview, IL, 2014), pp. 337–338.

[16]S. T. Thornton and A. Rex, *Modern physics for scientists and engineers* (Cengage Learning, Boston, MA, 2012), p. 103.

[17]D. Griffiths, *Introduction to electrodynamics*, 4th ed. (Pearson Education, Glenview, IL, 2014), p. 259.

[18]*Electron charge to mass quotient*, `https://physics.nist.gov/cgi-bin/cuu/Value?esme`.